PAPER • OPEN ACCESS

Tunability experiments at the FERMI@Elettra free-electron laser

New Journal of Physics
The open access journal for physics

Tunability experiments at the FERMI@Elettra free-electron laser

E Allaria[1], A Battistoni[1], F Bencivenga[1], R Borghes[1], C Callegari[1,2,10], F Capotondi[1], D Castronovo[1], P Cinquegrana[1], D Cocco[1,11], M Coreno[1,2], P Craievich[1,12], R Cucini[1], F D'Amico[1], M B Danailov[1], A Demidovich[1], G De Ninno[1,3], A Di Cicco[4], S Di Fonzo[1], M Di Fraia[1,5], S Di Mitri[1], B Diviacco[1], W M Fawley[1], E Ferrari[1], A Filipponi[6], L Froehlich[1], A Gessini[1], E Giangrisostomi[1], L Giannessi[1,7], D Giuressi[1], C Grazioli[1], R Gunnella[4], R Ivanov[1], B Mahieu[1,8], N Mahne[1], C Masciovecchio[1], I P Nikolov[1], G Passos[1], E Pedersoli[1], G Penco[1], E Principi[1], L Raimondi[1], R Sergo[1], P Sigalotti[1], C Spezzani[1], C Svetina[1], M Trovò[1] and M Zangrando[1,9]

[1] Elettra-Sincrotrone Trieste SCpA, Trieste, Italy
[2] CNR-IMIP, Monterotondo Scalo, Italy
[3] Laboratory of Quantum Optics, University of Nova Gorica, Nova Gorica, Slovenia
[4] Università di Camerino, Camerino, Italy
[5] Università di Trieste, Trieste, Italy
[6] Università degli studi dell'Aquila, L'Aquila, Italy
[7] ENEA C. R. Frascati, Frascati, Italy
[8] CEA Saclay, DSM/IRAMIS/SPAM, Gif-sur-Yvette, France
[9] CNR-IOM, Trieste, Italy
E-mail: carlo.callegari@elettra.trieste.it

New Journal of Physics **14** (2012) 113009 (19pp)
Received 20 September 2012
Published 7 November 2012
Online at http://www.njp.org/
doi:10.1088/1367-2630/14/11/113009

[10] Author to whom any correspondence should be addressed.
[11] Current address: SLAC National Accelerator Laboratory, Menlo Park, CA, USA.
[12] Current address: Paul Scherrer Institut, Villigen, Switzerland.

Abstract. FERMI@Elettra is a free electron-laser (FEL)-based user facility that, after two years of commissioning, started preliminary users' dedicated runs in 2011. At variance with other FEL user facilities, FERMI@Elettra has been designed to deliver improved spectral stability and longitudinal coherence. The adopted scheme, which uses an external laser to initiate the FEL process, has been demonstrated to be capable of generating FEL pulses close to the Fourier transform limit. We report on the first instance of FEL wavelength tuning, both in a narrow and in a large spectral range (fine- and coarse-tuning). We also report on two different experiments that have been performed exploiting such FEL tuning. We used fine-tuning to scan across the 1s–4p resonance in He atoms, at ≈23.74 eV (52.2 nm), detecting both UV–visible fluorescence (4p–2s, 400 nm) and EUV fluorescence (4p–1s, 52.2 nm). We used coarse-tuning to scan the $M_{4,5}$ absorption edge of Ge (∼29.5 eV) in the wavelength region 30–60 nm, measured in transmission geometry with a thermopile positioned on the rear side of a Ge thin foil.

Contents

1. Introduction

Free-electron lasers (FELs) [1] use coherent emission from relativistic electrons passing through an undulator to generate high-intensity photon pulses that can have peak brightness several orders of magnitude larger than the one typically available from synchrotron light sources. In FELs, the electrons are forced to emit coherently by prolonged interaction with the electromagnetic field emitted within the undulator. If a resonance condition between the

electron beam and the electromagnetic field is established, then energy transfer from the field to the electrons and vice versa induces a modulation of the electron beam energy that is then converted into a spatial modulation with the same periodicity as the electromagnetic wavelength. The periodically bunched electrons emit coherently, allowing a strong amplification of the initial electromagnetic field. The recent extension of the tuning range of FELs to the x-ray spectral region [2] has created great opportunities for science, as is witnessed by the number of x-ray user facilities that are coming online.

FERMI@Elettra is an FEL-based user facility that, after two years of commissioning, started preliminary users' dedicated runs in 2011 [3]. A distinguishing feature of FERMI@Elettra, with respect to other facilities [4–6], is the design aimed at improving spectral stability and longitudinal coherence, through the use of an external laser initiating the FEL process [7, 8].

While the resonant emission process of a relativistic beam in an undulator is similar in FELs and synchrotrons, the nonlinear coupling in FELs, which is responsible for the gain process, creates a number of constraints on the electron beam properties, on alignments and on the overall machine operability. In particular, the simple operation of tuning of the source wavelength, which in synchrotrons is nowadays a parameter easily changed by the users according to their experimental needs, is for FELs a proposition that may require some additional effort.

In the case of oscillator FELs [1, 9], mostly used in the IR and visible portion of the electromagnetic spectrum, tuning must contend with the reflectivity of the mirrors that compose the optical cavity, which is generally a function dependent on the operation wavelength. At shorter wavelengths (VUV–x-ray) the limitations imposed by the mirrors may be solved with single-pass high-gain FEL configurations [10]. In this case, the lasing scheme is based on self-amplified spontaneous emission (SASE), and the necessity to vary the resonance condition in a long undulator system may still affect the electron beam properties, leading to a reduction of the FEL gain and efficiency.

In addition, in SASE, the gain process predominantly amplifies the electron beam shot noise, typically by a factor of $\sim 10^8$, introducing considerable intrinsic randomness in the fundamental pulse properties (timing, intensity, longitudinal coherence, temporal and spectral profile). These intrinsic fluctuations are virtually suppressed in a seeded FEL, such as FERMI@Elettra, where the process is initiated by the highly coherent seed generated by an external source, which is then multiplied in frequency to reach the desired spectral range [11, 12].

In a seeded machine, frequency tuning requires the simultaneous change of two parameters, namely the seed wavelength and the resonance condition in the undulator. The additional effort is compensated for by the lower gain needed ($\sim 10^3$) and by the excellent properties of the emitted pulse, but efficient exploitation of the improved spectral purity requires precise control of the emission wavelength.

In this paper, we explore the FEL tuning scheme adopted for FERMI@Elettra. We report on the first instance of wavelength tuning of a short-wavelength FEL facility, both in a narrow and in a large spectral range (fine- and coarse-tuning). We also report on two different experiments, where fine- and coarse-tuning are exploited to scan across an atomic resonance and an elemental absorption edge, respectively.

The paper is organized as follows. Section 2 describes the FEL FERMI@Elettra. Section 3 is devoted to an overview of the principles of the high-gain harmonic generation (HGHG)

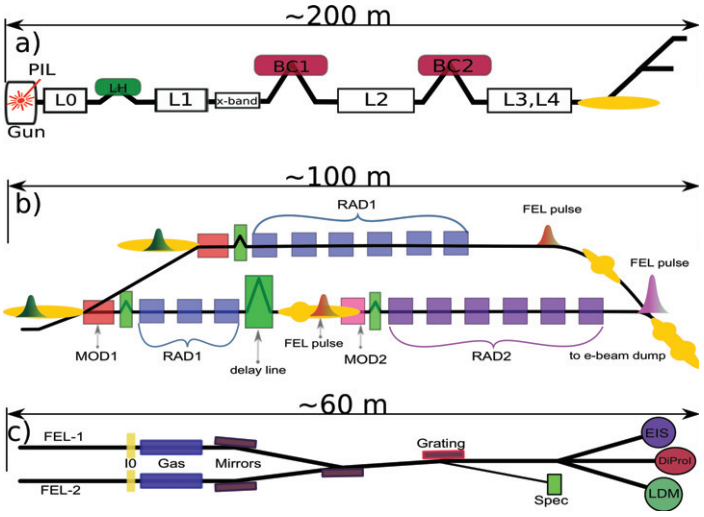

Figure 1. Schematic sketch of the FERMI@Elettra FEL with (a) the electron beam accelerator (LINAC), (b) the undulator section and (c) the experimental hall including the photon beam transport to the experimental stations (PADReS).

seeding scheme, adopted for FERMI@Elettra. Section 4 describes the procedures to tune the FEL for fine (section 4.1) and coarse (section 4.2) wavelength scans. Section 5 describes the photon transport system and the associated diagnostics. Finally, section 6 reports on the fine scan across the atomic He 1s–4p resonance and section 7 describes the coarse scan across the $M_{4,5}$ absorption edge of a thin Ge film.

2. The FERMI@Elettra free-electron lasers

FERMI@Elettra is an FEL user facility in operation at Elettra-Sincrotrone Trieste (Italy) that has been designed for experiments in the VUV–soft x-ray spectral range [7]. FERMI@Elettra is based on two FEL beamlines that share the electron beam produced by a common linear accelerator (LINAC). It has been designed to produce sub-ps pulses in the wavelength range from 80 nm down to 4 nm with gigawatt peak power. The use of an external seed to initiate the FEL process allows FERMI@Elettra to improve the longitudinal coherence compared to existing FEL facilities that operate in the same spectral range. FERMI@Elettra in optimized conditions is capable of producing FEL pulses close to the Fourier time-bandwidth limit, as confirmed by first results [3].

The layout of the machine can be divided into three main parts (figure 1): the accelerator, where electrons are produced and brought to the design energy; the undulator, where FEL radiation is generated; and the experimental hall, where the FEL beam is characterized and focused into the experimental chambers (currently three beamlines are in operation at FERMI: DiProI, EIS and LDM [8]). A photo-cathode RF gun [13] produces an electron bunch of charge about 500 pC, 8 ps long (full-width at half-maximum (FWHM)) and a normalized emittance <1 mm mrad. Electron bunches are then accelerated in the LINAC by S-band normal-conducting accelerating structures. The final energy reached at the end of the LINAC can be varied from 0.9 to about 1.3 GeV. Two magnetic compressors (BC1 located at approximately one third and BC2 at two thirds of the LINAC length) at about 700 MeV, allow us to increase the electron beam peak current to the value required for optimal operation of the FELs.

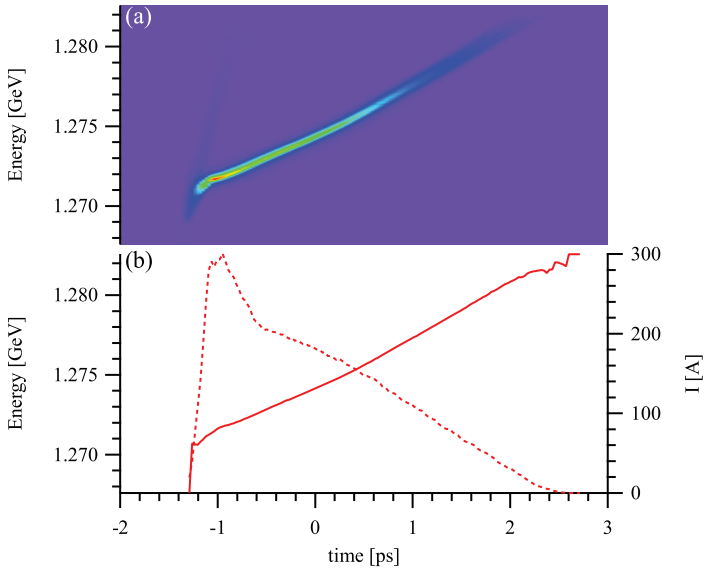

Figure 2. (a) Electron beam phase space measured at the end of the LINAC. (b) Energy profile (full curve, left axis) and current profile (dashed curve, right axis) versus time for the electron beam of FERMI@Elettra, exhibiting the characteristic phase space for a nonlinearly compressed beam.

A so-called laser heater [14] and a fourth-harmonic RF-cavity operating at X-band frequency are used to manipulate the electron beam longitudinal phase space for optimum FEL gain. These components were still under commissioning and were not used during the experiments reported here. As a consequence, electron beam parameters such as energy and current could not be made as independent of the position along the bunch as desired.

In particular, the measured current profile exhibits a typical spike on the head, followed by a slowly decreasing tail (figure 2). Similarly, the electron beam energy changes all along the bunch, with a marked chirp. It is important to remark that in the case of FERMI@Elettra, the FEL pulse is not necessarily generated by the current spike, but occurs at that portion of the electron bunch which has interacted with the seed laser. This region is substantially shorter than the electron bunch itself and its position is optimized a few hundreds of femtoseconds behind the main current spike.

To cover the wide design spectral range, FERMI@Elettra has been divided into two independent FELs, which share the same electron beam in a mutually exclusive manner. FEL-1, used in the study presented here, covers the spectral range from 80 nm down to 20 nm. FEL-2, currently under installation, will cover the range from 20 nm down to 4 nm. Both FELs are seeded and based on the HGHG scheme [12] described in section 3. FEL-1 features a total of seven undulators. The first one is the modulator: a 3 m long planar undulator with a 10 cm period and a variable gap necessary to define the desired resonance condition between the electron beam and the external UV seed laser. The successive radiator consists of six APPLE-II [15] undulators 2.4 m long with a period of 5.5 cm. The use of APPLE-II undulators allows FERMI@Elettra to produce FEL photons with variable polarization that can be changed from linear to circular according to user requirements. FEL-2, in order to cover the higher photon energy spectral range, down to 4 nm (60th harmonic of the external seed), uses a double HGHG

cascade [7]. The first stage is a replica of the undulators of FEL-1; the final radiator uses six APPLE-II undulators with a 3.5 cm period.

In both FELs the HGHG process is initiated by an external UV seed laser which is described in section 3.1. The chosen laser provides short pulses of the order of 150 fs (FWHM) with an energy per pulse that can be varied up to about 50 μJ. The seed laser uses an optical parametric amplifier (OPA) in order to allow a continuous change in the laser wavelength, which in the configuration used can be varied from 230 to 260 nm.

A critical point for seeded FELs such as FERMI@Elettra is the control of the synchronization of the electron beam and the seed laser, since the FEL process relies on the interaction between the two. An innovative timing distribution system [16] has been designed and implemented for FERMI@Elettra that allows us to have less than 100 fs rms jitter between the electron beam and the external seed laser in the undulators.

The photon diagnostic and delivery system, described in section 5, has been designed so that any one of the three beamlines can use the radiation produced by either FEL.

3. High-gain harmonic generation

FERMI@Elettra has been designed based on the HGHG scheme [12]. In HGHG the electron beam is first coherently bunched at the desired wavelength, then sent into a long radiator where coherent emission occurs and is amplified by the forthcoming FEL process. The HGHG scheme produces bunching through the interaction of the electron beam with the seed laser: in the modulator, the seed laser produces an energy modulation at its own wavelength of operation, which is converted into a charge density modulation (bunching) when the beam passes through a magnetic chicane. Depending on the setting of the chicane the bunching can also be optimized for a selected harmonic of the external laser [12, 17, 18]. Recently, it was shown that FERMI@Elettra can be efficiently operated up to the 13th harmonic of the UV seed laser (260–200 nm) [3], while coherent emission has been observed up to the 65th harmonic [19].

The main benefit of HGHG FELs with respect to the commonly used SASE scheme is the capability to control the longitudinal coherence of the pulse and to provide narrow-bandwidth FEL pulses. In the case of SASE, due to the noise that initializes the process, pulses are generally composed of several very short spikes, appearing in both the time and spectral domains. A FEL saturation, the output SASE bandwidth is determined by the relative width of the FEL gain curve, whose rms value is of the order of the FEL ρ parameter [10]. The latter is a function of the electron beam and undulator parameters, and is generally $\sim 10^{-3}$ for soft x-ray FELs and a few 10^{-4} for hard x-ray FELs. In the case of FERMI@Elettra, ρ is estimated to be about 1.3×10^{-3} and corresponds to the rms bandwidth expected in the SASE mode. In an HGHG FEL, both the temporal and spectral properties of the FEL are closely related to those of the seed laser. An HGHG FEL is thus able to generate FEL pulses exhibiting a well-defined temporal profile, which at FERMI@Elettra is expected to be $\sim$100 fs long with a bandwidth of the order of a few tens of meV. If HGHG is used to generate very high harmonics, a pulse shortening and bandwidth increase are expected for the FEL pulse relative to the seed pulse [20], due to the nonlinear process that generates the bunching. In the range explored by FEL-1, however, such an effect is limited.

Because the FEL process is initiated by the external seed laser, the wavelength of an HGHG FEL is strictly defined by the wavelength of the external laser [21], and changing the latter is

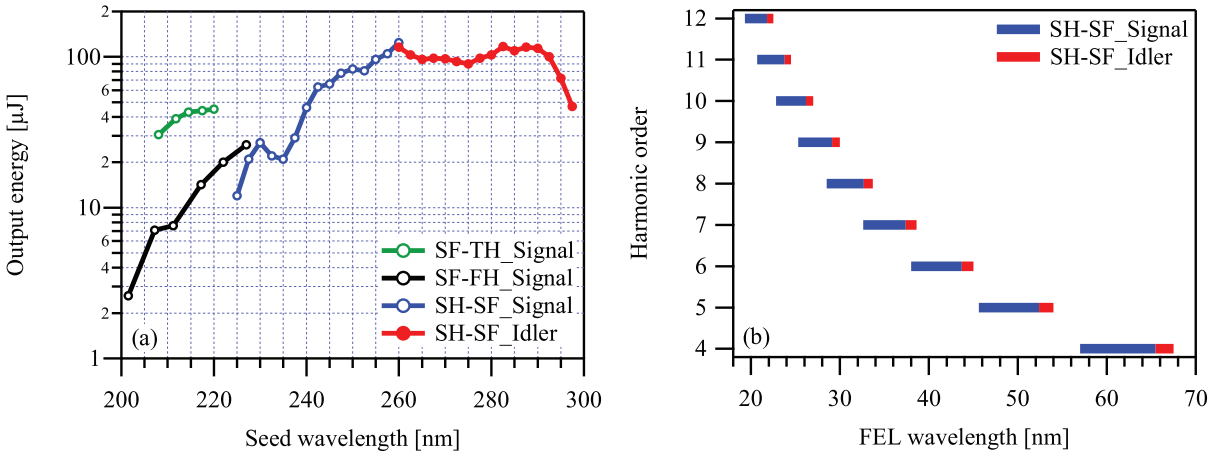

Figure 3. (a) Seed laser tunability curves. (b) Coverage of the 20–66 nm tuning range through different FEL harmonics seeded by two of the ranges of the OPA.

the simplest way to tune the FEL. An alternative way has been proposed that takes advantage of the process that is responsible for the bunching [22, 23].

3.1. The seed laser

Details of the exact layout and parameters of the FERMI@Elettra seed laser can be found elsewhere [24]. Here we will only summarize its main features briefly. An extensive computer simulation campaign has been performed at the early stages of the FERMI@Elettra design to obtain a set of starting parameters for the seed laser system. It was found that a broadly tunable deep-UV pulse (wavelength range 200–300 nm) having a peak power of the order of 100 MW is needed in order to obtain strong enough bunching. The seed pulse duration has been chosen in the 100–200 fs range, leading therefore to the need to have about 10–20 μJ of UV energy per pulse reaching the modulator. In the broadly tunable version, which is expected to become the main mode of operation after completion of the commissioning, the only feasible solution was to use an optical parametric amplifier (OPA). The implemented one is a Light Conversion/Coherent Opera Solo. It is pumped by a 3.3 mJ femtosecond regenerative amplifier (Coherent Elite), which was later upgraded at Elettra-Sincrotrone Trieste to reach 6.5 mJ per pulse by adding a single-pass amplifier stage. The signal and idler waves of the OPA span from 1.08 to about 2.6 μm; up-conversion to UV is achieved through a sequence of nonlinear harmonic generation and mixing. The OPA output energy per pulse in the spectral range that can be used for seeding the FEL is shown in figure 3(a). The optical beam transport from the seed laser table to the undulator is rather long and complex, and efforts have been made to find a proper multilayer system that would cover a range as wide as possible with losses as small as possible. In the currently installed version, the overall optical transport loss (reflective telescope and 8–10 folding and steering mirrors) is about 40% and allows us to deliver to the FEL sufficient seeding power in the 215–275 nm range.

As can be seen from figure 3(a), four different up-conversion processes have to be used in order to cover this range. So far, due to limited time, only one of them, namely SH SF-Signal (second harmonic of the frequency-mixed OPA signal and fundamental 780 nm light, the blue curve in figure 3(a)) has been used during FEL operation, with the seed laser tunable with sufficient power in the 228–262 nm range. The corresponding ranges of FEL tunability

achievable by choosing different FEL harmonics are shown in figure 3(b) by blue bars. A simple procedure taking a few minutes (not yet tested during FEL operation) allows us to switch to the other mixing process giving longer OPA wavelengths, which extends the FEL tunability ranges as shown by red bars in figure 3(b). For applications where the FEL wavelength does not need to be fully tunable there is the possibility to use as a seed the third harmonic (TH) of the Ti:sapphire amplifier. In this mode, different FEL wavelengths can still be obtained by switching between the different FEL harmonics (4th–13th demonstrated so far). In addition, the FEL wavelength in this mode can be tuned through fine-tuning of the seed wavelength, obtained by a precise rotation of the TH crystal angle. At present the UV range 260–262 nm can be covered in this way by the seed, so the FEL wavelength at each harmonic can be varied by about ±0.4%. In all cases, the seed laser wavelength is read by a tabletop spectrometer capable of determining the *absolute* seed wavelength within ≈0.1 nm uncertainty.

4. Free-electron laser tuning

As already mentioned, FEL emission occurs if the electron beam in the undulator is in resonance with the external electromagnetic field. The resonance condition is defined by the following equation:

$$\lambda = \lambda_w(1 + a_w^2)/(2\gamma^2), \tag{1}$$

where γ is the electron beam energy factor, λ is the resonant wavelength, λ_w is the period of the magnetic field in the undulator and a_w is the RMS value of the undulator magnetic strength parameter, typically in the range from 1 to 3 for FERMI@Elettra operation. The wavelength tuning of an FEL then requires the change of one of the parameters appearing in equation (1). Since the period of the undulator is constant, this means changing either the electron beam energy or the magnetic field strength. The former option is sometimes the only viable one for the case of fixed gap undulators with essentially constant field strength. FERMI@Elettra undulators have been designed to allow for the change of the magnetic strength by changing the undulator gap; this is the preferred solution as it does not require a change in the electron beam properties. In a seeded FEL, such as FERMI@Elettra, the final FEL wavelength is defined not only by the resonant condition but also by the seed laser wavelength λ_{SEED}. Undulator tuning has negligible impact on the final FEL wavelength but is very critical for maximum FEL power and for the spatial mode quality. The final FEL wavelength may be somewhat affected by the energy chirp of the electron beam [22] and only slightly by the resonance condition of the electron beam in the final radiator [21]. In the reported case, since the seeding is exploring only a small portion of the beam, the energy chirp can be considered as constant. The procedure adopted for tuning FERMI@Elettra is different for fine and large tuning since the wavelength steps are different in the two cases. In both cases, however, the resonance condition is changed by varying the undulator parameter and not the electron beam energy.

4.1. Fine-tuning

In the case of fine-tuning, the FEL has been tuned around 52.2 nm, which is the fifth harmonic of the seed laser at 261 nm; λ_{SEED} has been varied in steps of ∼0.1 nm, as reported in section 6. Such a small wavelength change (0.4%) is of the same order as the FEL ρ parameter; hence, the resonance condition is not completely lost after a change of λ_{SEED}. This allows one to keep the FEL lasing while the change is being performed; hence, only a quick optimization

of the undulator gap is necessary to restore the best resonance condition and to maximize the FEL power after the change in λ_{SEED}. It is also important to note that since the FEL continues to operate at the same harmonic of the seed, the optimal seed power and the optimal strength of the dispersion section do not change. The typical time required for the fine-tuning of FERMI@Elettra has been 5 min or less, mostly dictated by the change in the seed laser wavelength. Provided that the seed laser parameters are preserved while changing its wavelength, the FEL performance is uniform over the whole spectral range.

4.2. Coarse-tuning

By design, FERMI@Elettra can be tuned across the entire spectral range of FEL1 (80–20 nm) in a single session without the need to change the electron beam energy, only exploiting the capability to change the resonance condition by changing the undulator gaps. In our particular case, we chose the range of 60–30 nm within which we wanted to define an absorption edge by ten or more separate points. To cover such a large spectral range, one needs to concurrently change λ_{SEED} and the harmonic at which the FEL operates. For this reason the optimization is more complicated, and requires more time as compared to fine-tuning. To automate as much as possible the FEL tuning over a large spectral range, the seed laser has been prepared as described in section 3.1 so that λ_{SEED} could be changed from the FERMI@Elettra control system. The generally available seed laser wavelengths, the associated FEL wavelengths and FEL harmonics are reported in figure 3(b). A suitable combination of λ_{SEED} and FEL harmonic was chosen according to users' requests. Since the value of λ_{SEED} set with the OPA has some impact on the arrival time of the laser into the modulator, timing had to be adjusted after each change in order to properly overlap the seed laser pulse and the electron bunch. During these experiments, the FERMI@Elettra electron beam was characterized by a nonlinear current profile and energy profile in time (see figure 2), the above optimization was crucial and the final FEL performance, both in terms of stability and intensity, critically depended on it. After the optimization of the seeding, a new gap for the undulator has to be set in order to provide the resonance condition at the new FEL wavelength; the seed laser power and the strength of the dispersive section also have to be optimized for the new working point. Because all these procedures were not yet automated, the process generally required 15 min or more.

5. Photon transport and diagnostics

To manipulate and characterize the photon beam, and to transport it to the endstations, a dedicated Photon Analysis Delivery and Reduction System (PADReS) is installed at FERMI@Elettra [25]. By means of several diagnostic devices, PADReS provides important photon beam parameters to the users; in particular, the absolute intensity I_0, its spectral distribution $i_0(\lambda)$ and the central emission wavelength λ_{FEL} are available online, shot-to-shot, during the experiments; shots are identified system-wide with an 8-digit unique integer (bunch number). PADReS also includes the transport and refocusing of the photon beam into the end stations. While fine-tuning measurements, reported and discussed in section 6, were carried out using an unfocused beam at a vacuum chamber installed *ad hoc* halfway through the transport line, coarse-tuning measurements were carried out with a setup mounted inside the DiProI endstation [26]. The DiProI beamline operates with a Kirkpatrick–Baez (KB) [27] focusing system consisting of two active deformable optics [28] and capable of a design focusing (FWHM) of 6 μm $\times$ 8 μm at 52 nm.

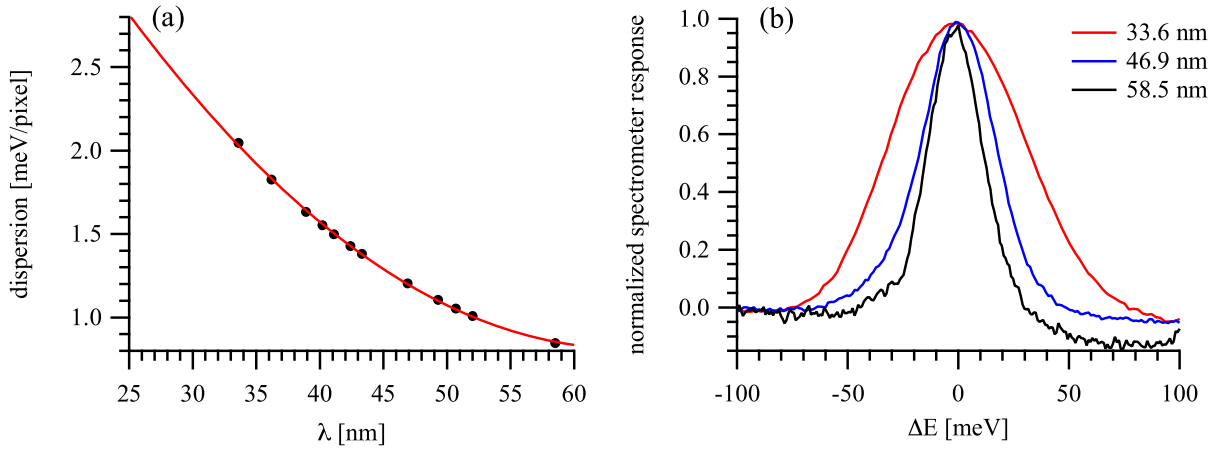

Figure 4. (a) Analytical function providing the dispersion curve of the PADReS spectrometer: $D(\lambda) = a\lambda^2 + b\lambda + c$, with $a = 1.3097 \times 10^{-3}$ meV pix^{-1} nm^{-2}, $b = -0.167\,88$ meV pix^{-1} nm^{-1} and $c = 6.1922$ meV pix^{-1}; with D given in meV pix^{-1} and λ in nm. (b) FEL spectral line shape for three different wavelengths.

5.1. Intensity monitor

The intensity monitor (in the following: I_0-monitor) is based on a simple ion chamber scheme, where the incoming radiation ionizes some rarefied gas (one of the noble gases or, as in the present case, N_2 at 3×10^{-3} Pa). The ion signal is then collected and measured shot-to-shot by a 20-bit-resolution picoammeter developed in-house (www.elettra.eu/lightsources/labs-and-services/instrumentation-and-detectors-lab); the value (expressed in arbitrary 'count' units, cts) is acquired, tagged with a unique bunch number and stored, by the centralized Tango-based system (www.tango-controls.org). We have verified the linear response of the I_0-monitor over a range going from 0 to ~30 000 cts, which easily covers the I_0-monitor counting interval spanned in the present experiment. Absolute calibration of the I_0-monitor is under way.

5.2. Energy spectrometer

The energy spectrometer is based on two variable line spacing (VLS) gratings, together capable of covering the entire photon energy range of FERMI@Elettra [25]. For the present measurements, a low-energy grating was used, as it covers the 100–24 nm range. The zeroth order, i.e. the specular reflection, carries ≈97% of the total intensity to the beamlines downstream, while the chosen diffraction order, usually the first, is focused onto a YAG crystal imaged by a CCD detector by means of the variable groove density of the VLS grating, whose position is controlled by a stepper motor and encoded by a Renishaw RGH24 readhead. In this way it is possible to obtain, online, the central wavelength λ_{FEL} and the spectral distribution $i_0(\lambda)$ of every single pulse, tagged by the bunch number. A typical value for the FWHM bandwidth at 52 nm is 0.07–0.08 nm, as measured experimentally during the commissioning of the instrument [29]. During the same commissioning, the absolute encoding of the spectrometer and its dispersion (meV per pixel or nm per pixel) have been calibrated against λ_{SEED} in the ranges shown in figure 4.

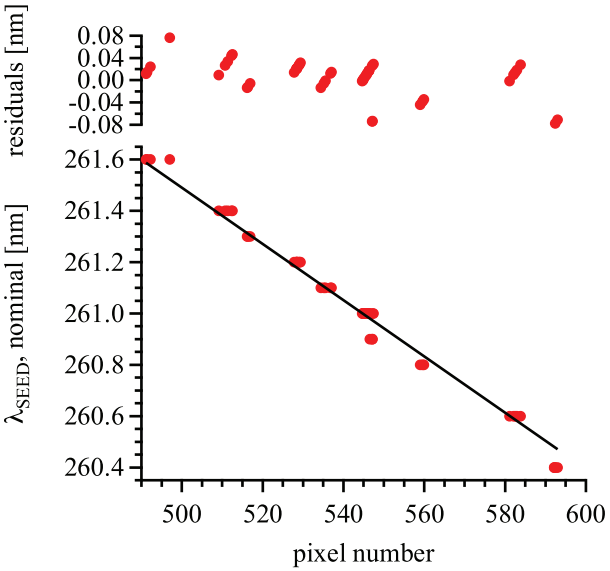

Figure 5. Fine-tuning calibration of the nominal seed-laser wavelength versus the peak center (pixel number).

5.2.1. Fine-tuning wavelength calibration. For the fine scans of the atomic resonance (section 6), a fresh calibration of the *absolute* reading of the PADReS spectrometer is performed by fitting the nominal seed laser wavelength with a straight line against the average peak position associated with a given dataset ($\bar{p}_{0,j}$; see section 6.2). The intercept is the only free parameter of the fit: the slope is kept fixed at the dispersion value determined above. This fit (figure 5) is used to calibrate the scale of the spectrometer itself, as well as to associate an average wavelength λ_j with each dataset.

6. Fine-tuning through an atomic resonance (He)

The sample of choice is helium, because of its simple electronic level structure and its large ionization potential, which lies above the lowest photon energy accessible to FERMI@Elettra. The energy-level scheme of the He atom, with excitation and fluorescent decay pathways, is shown in figure 6. According to the NIST database [30], the energy level separation for the 1s–4p transition of interest is $E = 23.742\,068\,9446$ eV, corresponding to a calculated wavelength of $\lambda = 52.221\,3086$ nm. Note that the *observed* wavelength has a slightly lower tabulated value (52.2186 nm); the difference is not relevant here.

Excitation of He from 1s (ground state) to 4p results in radiative decay through the following channels, among others: 4p–1s (direct, 52.2 nm) and 4p–2s (396.6 nm). Based on the respective Einstein coefficients, the branching ratio is $\approx 30:1$. Both the natural lifetime of the 4p state ($\approx$4 ns) and the response of the detectors (see figure 8) lie in the ns range and are thus much slower than the FEL pulse.

6.1. Experimental setup

The experimental setup consists of a six-way CF40 cross directly connected to the PADReS beamline. Helium gas was admitted into the chamber through a calibrated leak valve (Duniway).

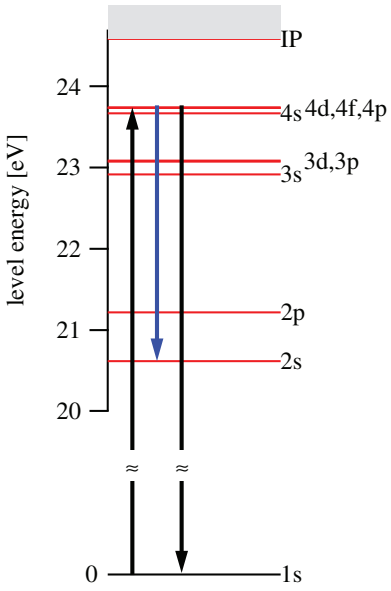

Figure 6. Energy-level scheme of the He atom, with excitation and fluorescent decay pathways of interest. Note that the d and f levels are indicated for completeness: transitions into them from the 1s ground state are electric-dipole forbidden. States above 4p have been omitted. IP stands for the ionization limit.

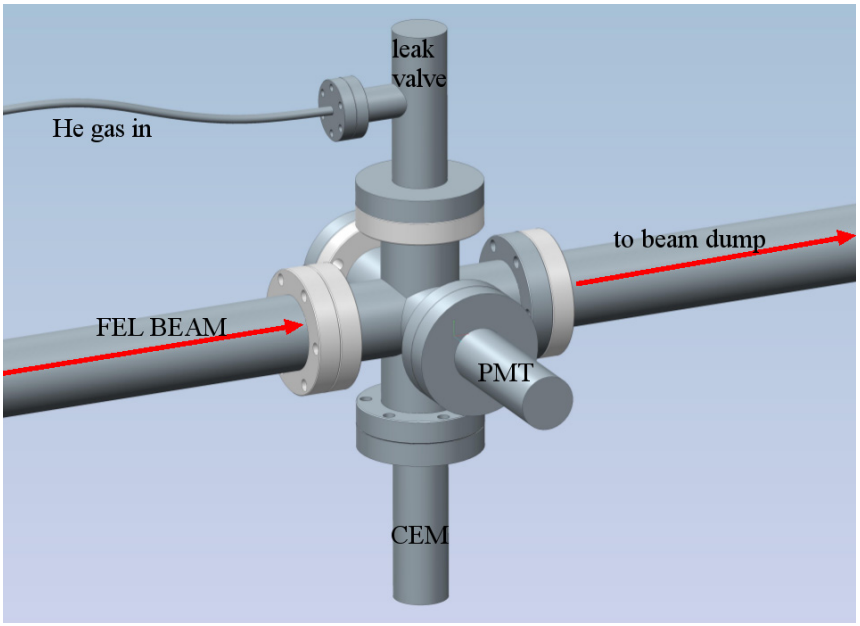

Figure 7. Schematic of experimental setup for section 6.

Under the operating conditions, the He pressure in the chamber was 1×10^{-6} Torr, as read by an ionization gauge (Pfeiffer, PKR261, uncorrected for He ionization efficiency).

A photomultiplier (PMT) and a channel electron multiplier (CEM) were mounted, perpendicular to the FEL beam, on separate arms of the cross, as indicated in figure 7. The CEM

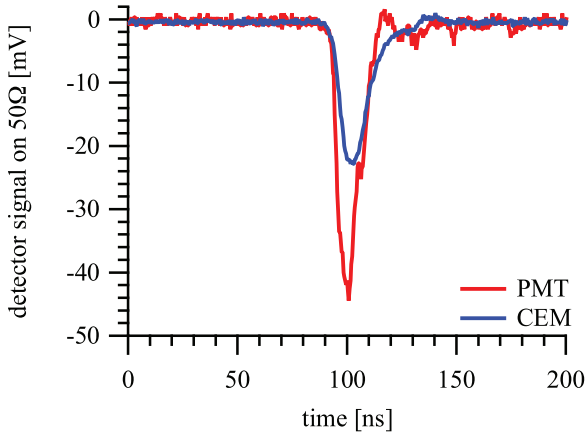

Figure 8. Typical pulses from PMT (red) and CEM (blue). Seed laser: 261.1 nm; I_0: 9014 cts.

was mounted in vacuum, while the PMT was attached outside a standard CF40 quartz window, and wrapped in a black cloth to shield it from ambient light. The PMT is a Hamamatsu R7899, with a sensitivity range of 300–650 nm. To further restrict its spectral sensitivity, a narrowband (40 nm) filter centered around 400 nm (Thorlabs FB400-40) was inserted between the PMT and the quartz window. The effects of the fluorescence induced by FEL photons hitting the chamber surface, the window or the filter itself have not been considered when designing the experiment; *a posteriori* the level of stray signal appears to be negligible. The PMT has been operated at a relatively low voltage of −753 V, corresponding to a nominal gain of $\sim 10^4$; the nominal quantum efficiency of the photocathode at 400 nm is ≈25 %.

The CEM is a Dr Sjuts GmbH KBL 10RS/90; it has been operated at −1692 V. We assume that each EUV photon reaching its surface will extract a few electrons which will be multiplied (nominal gain extrapolated from the available gain curves: 3×10^5).

The signals from the two detectors are digitized synchronously by two independent channels of a 600 MHz oscilloscope (LeCroy, waveSurfer 64Xs); each trace (figure 8) consists of 500 points spaced by 0.4 ns; $t = 0$ is arbitrarily set so that the peak is roughly centered on the scope screen. As already mentioned, the response of the detectors is slower than either the FEL pulse or the fluorescent decay of excited He atoms. In such a case the detector signal consists of a single pulse whose integrated area is (barring saturation effects) proportional to the number of excited atoms.

The traces are acquired shot-to-shot by the FERMI@Elettra centralized control and acquisition system (Tango-based (www.tango-controls.org)), along with the corresponding bunch number, I_0 reading and PADReS energy spectrum $i_0(\lambda)$.

6.2. Data reduction

A typical dataset consists of $i = 1$–n ($n = 3000$) shots, corresponding to 5 min of measuring time, during which all experimental settings (in particular, He pressure and FEL wavelength) are not changed by the experimenter. A valid dataset contains n I_0-monitor readings $\{I_{0,i}\}$; n pairs of oscilloscope traces which are integrated after baseline subtraction to obtain n peak areas $\{A_{\mathrm{CEM/PMT},i}\}$, n spectrometer traces (figure 10) each of which is fitted with a Gaussian

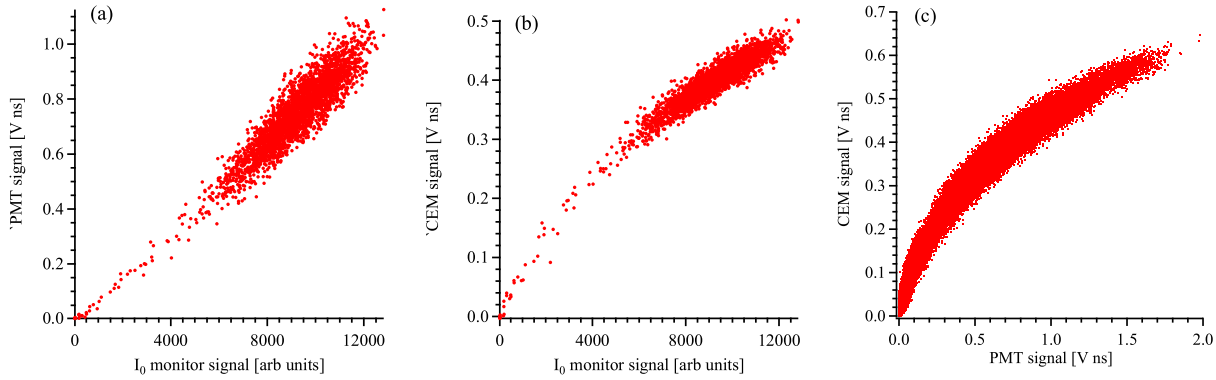

Figure 9. (a) Scatter plot of PMT and (b) CEM signal versus I_0 monitor signal, for one dataset at $\lambda_{\mathrm{SEED}} = 261.09$ nm. (c) Scatter plots of CEM signal versus PMT signal (all 51 datasets aggregated).

curve to obtain n peak positions $\{p_{0,i}\}$ (as pixel number). Because the fit process is automated, we must be able to reject the $p_{0,i}$ associated with poor fits, which we do by iteratively rejecting all outliers (values of $p_{0,i}$ differing by more than three standard deviations from the dataset average $\bar{p}_0 = (\sum_i p_{0,i})/n$; up to three rounds of outlier rejection may be necessary in a given dataset, but in most cases one is sufficient). We find that for a dataset of good quality (denoting stable operation of the FEL) the standard deviation of the peak position on PADReS spectrometer is 1–2 pixels. As the spectrometer is never moved during the present measurement, we can reasonably assume that its reading is a reliable indicator of the repeatability of the true wavelength.

Knowing $\bar{p}_{0,j}$ for each dataset (j: dataset index; 51 datasets total) and the calibration parameters of section 5.2.1, we calculate a wavelength λ_j. The set of points $(I_{0,i}, A_{\mathrm{PMT},i})_j$ in dataset j is fitted with a straight line forced to have zero intercept ($I_0 = m\, A_{\mathrm{PMT}}$) to extract the proportionality constant m_j. A plot of the pairs (λ_j, m_j) represents our atomic absorption line (figure 10). The profile is fitted with a Gaussian, giving a line center 52.218 nm consistent with the NIST value, and a FWHM of 0.06 nm slightly narrower than that measured by the PADReS spectrometer for a single shot. Because the natural width of the atomic line is $\sim 10^5$ times sharper than that of the FEL, the absorption profile reflects an average FEL linewidth.

6.2.1. Linearity of signal. As seen in figure 9(a) there is a good linearity relationship between I_0-monitor readings and PMT readings. It is then legitimate to identify the slope of the linear fit with the absorption at a given wavelength, obtaining the absorption profile of figure 10. The CEM signals, however, were saturating at high FEL intensities (figure 9(b)); we can rule out saturation of the atomic absorption or emission process, because the same effect would be observed with the PMT. Despite such inconvenience, the good correlation of the aggregated CEM data versus the PMT data (figure 9(c)) shows that the two methods are capable, as expected, of returning the same information provided that either the CEM data are suitably linearized or the measurement is repeated at lower CEM signal.

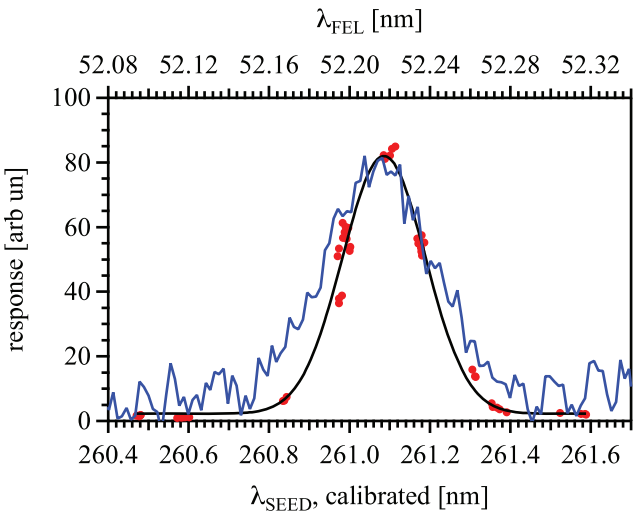

Figure 10. Reconstructed He absorption profile (red dots: PMT response versus calibrated wavelength; black line: Gaussian fit) and comparison with a PADReS single-shot spectrometer trace (blue line). Note that $\lambda_{FEL} = \lambda_{SEED}/5$.

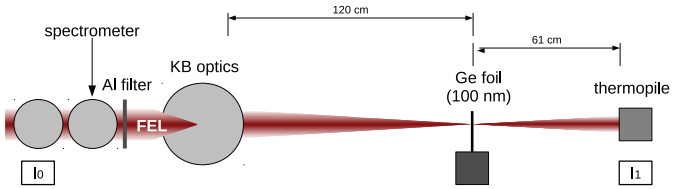

Figure 11. Schematic of the experimental setup for section 7.

7. Coarse-tuning through an absorption edge (Ge)

7.1. Experiment

The experimental setup, installed inside the DiProI chamber, consists of a self-standing Ge foil (nominal thickness 100 nm, Lebow Company) mounted on a movable sample holder and a YBCO thermopile (Fortech HTS GmbH) [31] positioned on the rear side of the sample (see figure 11). The thermopile works at room temperature and is insensitive to temperature changes. Moreover, it combines a fast response time of a few tens of ns with linearity over 12 decades up to megawatts of power, delivering an output signal of 1 mV μJ^{-1} for short pulses [32].

The FEL has been focused by the available KB optics onto a spot of about 300 μm diameter. The Ge foil has been positioned on the focal plane of the KB optics. We observed a tangible vibratory motion of the sample foil upon FEL irradiation compatible with both thermal expansion of the thin foil and radiation pressure induced by the beam. However, that effect deserves further analysis in order to be clarified.

After about 1 h of almost continuous exposure to the beam, the sample was partially destroyed, probably as an effect of the above-mentioned FEL-induced deformation. Successive measurements were carried out on the remaining fraction of the sample (about 50%) limiting the temporal exposure to the beam. Moreover, an Al foil (nominal thickness 400 nm) has been

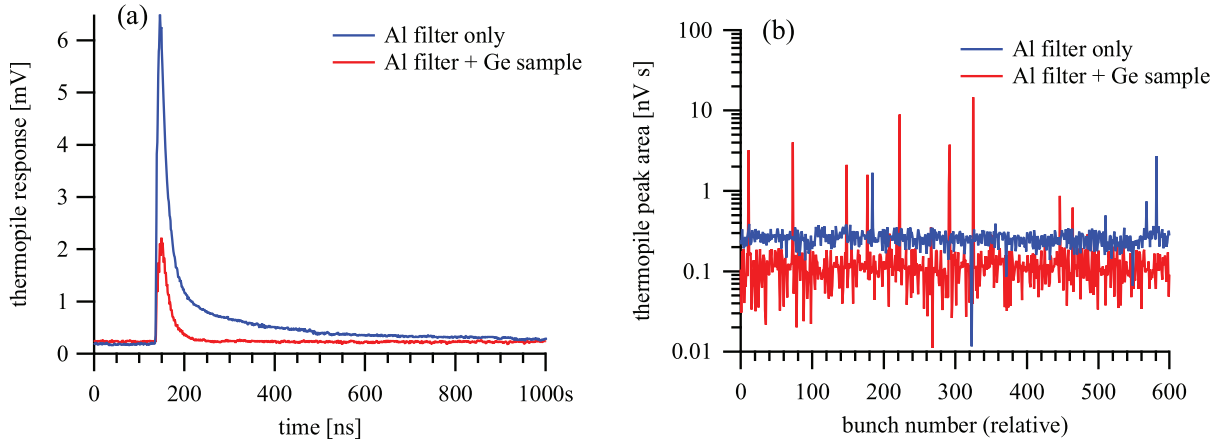

Figure 12. (a) Thermopile voltage swing subsequent to a single FEL pulse ($\lambda = 38.9$ nm). (b) Sequence of 600 thermopile counts (i.e. area under the voltage swing curve) at a repetition rate of 10 Hz, for $\lambda = 38.9$ nm.

used to attenuate the intensity of the FEL beam. As an immediate effect of the Al filter insertion, we observed the disappearance of the sample vibration.

The fraction of the FEL beam transmitted by the Ge sample has been calculated by the formula

$$T(\lambda) = \frac{\widetilde{I_1^{\mathrm{Ge}}}/\widetilde{I_0^{\mathrm{Ge}}}}{\widetilde{I_1}/\widetilde{I_0}}, \tag{2}$$

where I_1, I_0 are experimental quantities for a specific FEL wavelength, $\widetilde{\ }$ denotes the median of a set of 600 measurements and the presence (absence) of the superscript $^{\mathrm{Ge}}$ denotes the presence (absence) of the sample (in either case, with the Al filter inserted). Specifically, I_1 is given by the area under the curve $V(t)$ describing the thermopile voltage swing subsequent to the pulse absorption (see figure 12 (left)); I_0 indicates the I_0-monitor count (ionization chamber, PADReS) associated (the same bunch number) with I_1. A typical set of 600 measurements ($\lambda = 38.9$ nm, 1 min of data acquisition) of I_1 is shown in figure 12 (right). The FEL wavelength stability and spectral bandwidth have been monitored in real time and greatly exceed those required for the present measurement.

7.2. Results

A set of selected transmission measurements, carried out in a wavelength range including the Ge $M_{4,5}$-edge, is shown in figure 13. For comparison, the theoretical transmission curve [33] of a Ge foil (40 nm thickness) is superimposed on the experimental data points. The experimental data are in good agreement with the theoretical transmission profile; however, the above value of the Ge sample thickness appears to be significantly less than what is stated by the manufacturer (nominal thickness: 100 nm). This may be caused by the poor homogeneity of the sample (presence of cracks, holes or craters in the sample foil) and/or by a smaller effective overall thickness.

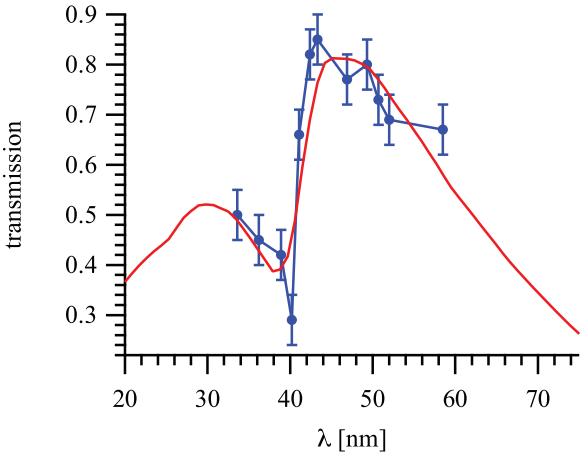

Figure 13. Theoretical transmission of a Ge foil of 40 nm thickness (solid line) compared with the experimental transmission data (dots) obtained with FERMI@Elettra in the Ge $M_{4,5}$-edge.

8. Summary and conclusions

We have reported on the first instance of FEL wavelength tuning, in both a narrow and in a large spectral range (fine- and coarse-tuning), as shown by the measurement of a sharp atomic resonance (He gas; 1s–4p transition) and a broad absorption edge (Ge foil; $M_{4,5}$-edge).

We thus experimentally confirm the fitness of FERMI@Elettra as a narrowband tunable light source that can be scanned continuously over a wide wavelength range (80–20 nm).

Acknowledgments

This work was partially supported by the Italian Ministry of University and Research under grant numbers FIRB-RBAP045JF2 and FIRB-RBAP06AWK3. CM acknowledges support from the European Research Council under the European Community Seventh Framework Program (FP7/2007-2013)/ERC IDEAS contract number 202804. GDN and MC acknowledge support from the Italian–Slovenian Crossborder Cooperation Programme, the CITIUS project (www.ita-slo.eu/projects/projects_2007_2013/2010090600115298). Thanks are due to Luca Romanzin for technical assistance in the installation of the fluorescence cell.

References

[1] Saldin E L, Schneidmiller E V and Michail V Yurkov 2000 *The Physics of Free Electron Lasers* (*Advanced Texts in Physics*) (Berlin: Springer)

[2] McNeil B W J and Thompson N R 2010 X-ray free-electron lasers *Nature Photon.* **4** 814

[3] Allaria E *et al* 2012 Highly coherent and stable pulses from the FERMI seeded free-electron laser in the extreme ultraviolet *Nature Photon.* **6** 699–704

[4] Ayvazyan V *et al* 2006 First operation of a free-electron laser generating GW power radiation at 32 nm wavelength *Eur. Phys. J.* D **37** 297
[5] Abela R *et al* 2006 XFEL: the European X-ray free-electron laser *Technical Design Report* (Hamburg: DESY)
[6] Pile D 2011 X-rays: first light from SACLA *Nature Photon.* **5** 456
[7] Bocchetta C *et al* 2007 FERMI@Elettra conceptual design report *Technical Report* ST/F-TN-07/12 (Sincrotrone Trieste)
[8] Allaria E, Callegari C, Cocco D, Fawley W M, Kiskinova M, Masciovecchio C and Parmigiani F 2010 The FERMI@Elettra free-electron-laser source for coherent x-ray physics: photon properties, beam transport system and applications *New J. Phys.* **12** 075002
[9] Deacon D A G, Elias L R, Madey J M J, Ramian J G, Schwettman H A and Smith T I 1977 First operation of a free-electron laser *Phys. Rev. Lett.* **38** 892
[10] Bonifacio R, Casagrande F, Cerchioni G, de Salvo Souza L, Pierini P and Piovella N 1990 Physics of the high-gain FEL and superradiance *Nuovo Cimento* **13** 1
[11] Boscolo I and Stagno V 1980 The converter and the transverse optical klystron *Nuovo Cimento* B **58** 267
[12] Yu L H 1991 Generation of intense UV radiation by subharmonically seeded single-pass free-electron lasers *Phys. Rev.* A **44** 5178
[13] Penco G *et al* 2012 Commissioning of the FERMI free electron laser photoinjector *Phys. Rev. STAB* submitted
[14] Spampinati S *et al* 2012 Commissioning of the FERMI@Elettra Laser heater *Proc. 2012 FEL Conf. (Nara, Japan)* MOPD58
[15] Sasaki S 1994 Analyses for a planar variably-polarizing undulator *Nucl. Instrum. Methods* A **347** 83
[16] Ferianis M, Bucconi A, Gaio G, Mian G, Predonzani M and Rossi F 2010 The copper free FERMI timing system: implementation and results *Proc. BIW10* (*Santa Fe, NM, 2010*) p 398
[17] Yu L H *et al* 2003 First ultraviolet high-gain harmonic-generation free-electron laser *Phys. Rev. Lett.* **91** 074801
[18] Allaria E and De Ninno G 2007 Soft-x-ray coherent radiation using a single-cascade free-electron laser *Phys. Rev. Lett.* **99** 014801
[19] Giannessi L *et al* 2012 *Proc. 2012 FEL Conf.* (*Nara, Japan*) MOOB6
[20] Ratner D, Fry A, Stupakov G and White W 2012 Laser phase errors in seeded free electron lasers *Phys. Rev. Spec. Top. Accel. Beams* **15** 030702
[21] Allaria E, Danailov M and De Ninno G 2010 Tunability of a seeded free electron laser through frequency pulling *Eur. Phys. Lett.* **89** 64005
[22] Shaftan T and Yu L H 2005 High-gain harmonic generation free-electron laser with variable wavelength *Phys. Rev.* E **71** 046501
[23] Doyuran A *et al* 2004 Chirped pulse amplification of HGHG-FEL at DUV-FEL facility at BNL *Nucl. Instrum. Methods* A **528** 467
[24] Danailov M B, Cinquegrana P, Demidovich A A, Ivanov R, Nikolov I and Sigalotti P 2011 Design and first experience with the FERMI seed laser *33rd Int. Free Electron Laser Conf.* ed J Chen, H Deng, L Liljeby, C Petit-Jean-Genaz, V R W Schaa, T Tanaka, H Yan and H Zen (Shanghai: SINAP) p 183
[25] Zangrando M *et al* 2009 The photon analysis, delivery, and reduction system at the FERMI@Elettra free electron laser user facility *Rev. Sci. Instrum.* **80** 113110
[26] Pedersoli E *et al* 2011 Multipurpose modular experimental station for the DiProI beamline of FERMI@Elettra free electron laser *Rev. Sci. Instrum.* **82** 043711
[27] Kirkpatrick P and Baez A V 1948 Formation of optical images by x-rays *J. Opt. Soc. Am.* **38** 766
[28] Cocco D, Bortoletto G, Sergo R, Sostero G and Cudin I 2010 A hybrid active optical system for wave front preservation and variable focal distance *Nucl. Instrum. Methods* A **616** 128
[29] Svetina C, Abrami A, Cudin I, Fava C, Gerusina S, Gobessi R, Rumiz L, Sostero G, Zangrando M and Cocco D 2011 Characterization of the FERMI@Elettra's on-line photon energy spectrometer *Advances in X-Ray/EUV Optics and Components VI* ed C Morawe, A M Khounsary and S Goto (*Proc. SPIE* vol 8139) (Bellingham: WA: SPIE) p 81390J

[30] Ralchenko Yu, Kramida A E and Reader J NIST atomic spectra database, v. 4.1.0 (online) www.nist.gov/pm1/data/asd

[31] Zeuner S, Prettl W and Lengfellner H 1995 Fast thermoelectric response of normal state $YBa_2Cu_3O_{7-\delta}$ films *Appl. Phys. Lett.* **66** 1833

[32] Treusch R, Lokajczyk T, Xu W, Jastrow U, Hahn U, Bittner L and Feldhaus J 2000 Development of photon beam diagnostics for VUV radiation from a SASE FEL *Nucl. Instrum. Methods* A **445** 456

[33] Henke B L, Gullikson E M and Davis J C 1993 X-ray interactions: photoabsorption, scattering, transmission, and reflection at $E = 50$–30000 eV, $Z = 1$–92 *At. Data Nucl. Data Tables* **54** 181